Theory of thermal transport in multilayer hexagonal boron nitride and nanotubes

L. Lindsay[1,*] and D. A. Broido[2]

[1]*Naval Research Laboratory, Washington, DC 20375, USA*
[2]*Department of Physics, Boston College, Chestnut Hill, Massachusetts 02467, USA*

We present a theory for the lattice thermal conductivity κ_L of single-walled boron nitride nanotubes (BNNTs) and multilayer hexagonal boron nitride (MLBN), which is based on an exact numerical solution of the phonon Boltzmann equation. Coupling between layers in MLBN and nanotube curvature in BNNTs each break a phonon scattering selection rule found in single-layer hexagonal boron nitride (SLBN), which reduces κ_L in these systems. We show that out-of-plane flexural phonons in MLBN and out-of-tube phonons in BNNTs provide large contributions to κ_L, qualitatively similar to multilayer graphene (MLG) and single-walled carbon nanotubes (SWCNTs). However, we find that the κ_L's in BNNTs and MLBN are considerably smaller compared to similar SWCNTs and MLG structures because of stronger anharmonic phonon scattering in the former. A large and strongly temperature-dependent isotope effect is found reflecting the interplay between anharmonic and isotope scattering phonons. Finally, we also demonstrate convergence of BNNTs into SLBN for large-diameter nanotubes and MLBN to bulk hexagonal boron nitride within a few layers.

I. INTRODUCTION

Like the more intensely studied graphene and single-walled carbon nanotubes (SWCNTs), boron nitride can be constructed into single or layered sp^2-bonded hexagonally packed planes and into nanotubes with alternately bonded boron and nitrogen atoms instead of carbon. Despite having similar lattice constants, unit cell masses, and phonon dispersions,[1–7] the measured lattice thermal conductivity κ_L of bulk hexagonal boron nitride (h-BN) is a fifth that of graphite.[8,9] Qualitatively consistent with this, molecular dynamics (MD) simulations of κ_L for boron nitride nanoribbons and small-diameter single-walled boron nitride nanotubes (BNNTs) find significantly lower values than their carbon-based counterparts.[10] On the other hand, recent measurements of κ_L for isotopically enriched multiwalled boron nitride nanotubes show similar values to multiwalled carbon nanotubes.[11]

In order to shed light on this issue and develop a more comprehensive understanding of h-BN systems, we present a Boltzmann transport equation (BTE) theory for κ_L of BNNTs and multilayer hexagonal boron nitride (MLBN), which includes anharmonic phonon-phonon and isotopic impurity scattering. We find that intrinsic phonon-phonon scattering selection rules play important roles in determining κ_L, similar to the case of SWCNTs and multilayer graphene (MLG).[12–14] In particular, we show that out-of-plane vibrations in MLBN and out-of-tube vibrations in BNNTs provide large contributions to κ_L, and the interaction between layers in MLBN and nanotube curvature in BNNTs violate a 2D selection rule in SLBN, leading to a substantial reduction in κ_L. However, we find stronger anharmonic three-phonon scattering in MLBN and BNNTs, which is responsible for the lower κ_L compared to MLG and SWCNTs. This finding is also supported by previous results found for SLBN and h-BN.[15] Calculated enhancements to κ_L are found to be relatively strong for isotopically pure BNNTs (20–30%) around room temperature, although somewhat less than those reported for multiwalled BNNTs in Ref. 11 (∼50%). We also find a strong temperature dependence to the isotope effect reflecting the

interplay between anharmonic and isotope scattering. We show that with increasing diameter $\kappa_{\mathrm{BNNT}} \to \kappa_{\mathrm{SLBN}}$ and with increasing layer number, N, $\kappa_{\mathrm{MLBN}} \to \kappa_{\mathrm{hBN}}$.

Sec. II provides an overview of the phonon properties and three-phonon selection rules relevant in BNNTs, SLBN, and MLBN. In Sec. III, we discuss the lattice thermal conductivities of different h-BN systems. Our results for the lattice thermal conductivities and subsequent discussion are presented in Sec. IV. We also discuss other recent theoretical predictions in relation to this work in Sec. IV. In Sec. V, we give a summary of this work and our conclusions. Appendix A provides a detailed account of the phonon-phonon scattering selection rules, while Appendix B outlines the details of the relevant scattering mechanisms and the Boltzmann transport equation.

II. PHONONS AND SCATTERING SELECTION RULES

An accurate representation of the interactions between atoms is required to effectively model the thermal transport in h-BN systems. Phonon frequencies ω_λ and acoustic phonon velocities $v_{\lambda\alpha} = d\omega_\lambda/dq_\alpha$ are determined from the harmonic interatomic force constants (IFCs), while anharmonic IFCs are essential for describing intrinsic phonon-phonon scattering.[16] Here, $\lambda = (\vec{q}, j)$ designates a phonon with wave vector $\vec{q}$ in branch j, and α is a Cartesian component. For h-BN, $\vec{q}$ is a 3D wave vector, and $j = 1, \ldots, 12,$[14,15] for SLBN and MLBN, $\vec{q}$ is a 2D wave vector in the plane of the layers with $j = 1, \ldots, 6N$.[14,15,17] In BNNTs, $\vec{q} = (q, l)$ where q is a continuous wave vector along the nanotube axis, l is an angular quantum number, and $j = 1, \ldots, 6$.[12,13] The phonon frequencies are determined by diagonalization of the dynamical matrix:

$$D_{\alpha\beta}^{\kappa\kappa'}(\vec{q}) = \frac{1}{\sqrt{m_\kappa m_{\kappa'}}} \sum_{\ell'\delta} \Phi_{\alpha\delta}^{0\kappa,\ell'\kappa'} S_{\delta\beta}^{\ell'} e^{i\vec{q}\vec{R}_{\ell'}} \qquad (1)$$

for a given $\vec{q}$ in the Brillouin zone of an h-BN system. Here, $\ell\kappa$ designates the κth atom in the ℓth unit cell, m_κ is the mass of the κth atom, and α, β, and δ are Cartesian components. Here, $\vec{R}_\ell$

is the lattice vector for the ℓth unit cell in Cartesian components for SLBN, MLBN, and h-BN. In BNNTs, $\vec{R}_\ell = (\theta_\ell, z_\ell)$ with θ_ℓ and z_ℓ specifying the coordinates around the nanotube axis and along the axis, respectively.[12,13,18] In Eq. (1), $S_{\delta\beta}^\ell$ is a rotation matrix for the ℓth unit cell in BNNTs and the identity matrix for the other systems. The harmonic IFCs, $\Phi_{\alpha\beta}^{\ell\kappa,\ell'\kappa'} = \frac{\partial^2 \Phi}{\partial u_\alpha^{\ell\kappa} \partial u_\beta^{\ell'\kappa'}}|_0$, with $u_\alpha^{\ell\kappa}$ being atomic displacements from equilibrium, are determined by a given interatomic potential energy, Φ.

For the weak interlayer bonding in MLBN, we use a Lennard–Jones potential $V_{LJ}(r_{ij}) = 4\varepsilon[(\sigma/r_{ij})^{12} - (\sigma/r_{ij})^6]$ where ε and σ are adjusted to best fit the interplanar distance and c-axis phonon dispersion, and r_{ij} is the distance between atoms i and j in adjacent layers. We consider coupling between nearest planes with AA' stacking consistent with *ab initio* calculations.[19] For the in-plane covalent bonding, we employ a Tersoff empirical interatomic potential[20,21] with parameters optimized to best fit harmonic phonon properties of h-BN.[15] The Tersoff potential has been successfully used to model thermal transport properties of graphene, SWCNTs, SLBN, and BNNTs.[10,12–15,17,22–25]

For SLBN and MLBN, the Tersoff parameters presented in Ref. 15 accurately represent the quadratic out-of-plane acoustic (ZA_1) phonon branch and give velocities for the linear transverse and longitudinal acoustic (TA_1 and LA_1) branches within 5% of experiment.[7] These branches provide the dominant contributions to κ_L so their accurate description is most important. There is not as good agreement with the higher-frequency optical modes, in part due to our neglect of the slightly ionic bonding of B and N atoms. However, we find that around room temperature, the optic branches in h-BN and graphene systems play only a small role in thermal transport, justifying this approximation. The effect on the acoustic branches due to ionicity has been shown to be negligible.[26] Recently, a similar Tersoff parameterization used for MD calculations of SLBN and BNNTs also demonstrates good agreement with the experimental in-plane h-BN phonon dispersion.[10]

For MLBN, the weak interlayer coupling produces N-1 low-lying optic phonon branches (one for h-BN) for each acoustic branch, labeled $ZA_{i>1}$, $TA_{i>1}$, and $LA_{i>1}$.[14] The flexural branches $ZA_{i>1}$ significantly deviate from the ZA_1, while the $TA_{i>1}$ and $LA_{i>1}$ branches are degenerate with the TA_1 and LA_1 except very near the Γ point, (see Fig. 1 in Ref. 14). Multilayer hexagonal boron nitride has $3N$ optic branches little affected by the weak interlayer coupling, which are degenerate with the six optical branches of h-BN. In BNNTs, there are four acoustic branches, linear torsional and longitudinal acoustic branches ($l = 0$, $j = 2$ and 3) and two quadratic flexure branches ($l = \pm 1$, $j = 1$), as well as numerous optic branches.[12,13] For a given l, the $j = 1$ phonon branches correspond to low-frequency out-of-tube vibrations, the radial breathing mode ($l = 0$, $j = 1$) being one. The $j = 2$ and 3 branches correspond to low-frequency in-tube vibrations.

Intrinsic phonon-phonon scattering is the dominant cause for thermal resistance to heat flow in semiconductors, such as h-BN systems, around and above room temperature.[16] In this paper, we consider three-phonon scattering processes and scattering selection rules which play critical roles in understanding κ_L of BNNTs, SLBN, and MLBN. The phase space for
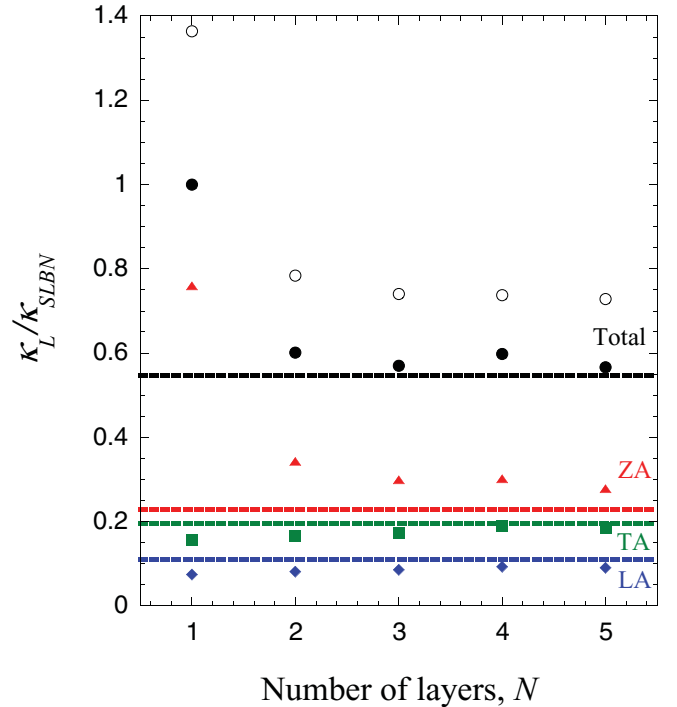

FIG. 1. (Color online) Calculated κ_L for MLBN vs layer number (solid black circles). Also shown are the per-branch contributions for ZA (red triangles), TA (green squares), and LA (blue diamonds) branches. The corresponding estimated h-BN values are shown by the horizontal dashed lines. The calculated κ_L for isotopically pure MLBN is also shown (hollow black circles). For all cases, $L = 10\,\mu m$ and $T = 300$ K.

three-phonon scattering is defined from all processes satisfying the conservation of energy and momentum: $\omega_j(\vec{q}) \pm \omega_{j'}(\vec{q}') = \omega_{j''}(\vec{q}'')$ and $\vec{q} \pm \vec{q}' = \vec{q}'' + \vec{K}$, where $\vec{K}$ is a reciprocal lattice vector, which is zero for normal processes and nonzero for Umklapp processes, and the $\pm$ signs correspond to the two types of possible three-phonon processes.[16]

In BNNTs where $\vec{q} = (q, l)$, conservation of crystal momentum in a three-phonon scattering process not only restricts the translational wave vectors q, but also imposes a restriction on the azimuthal quantum numbers l, which is discussed in Appendix A and in Refs. 12 and 13. This azimuthal selection rule severely limits the number of three-phonon scattering processes allowed and has permitted rigorous calculations of large diameter chiral and achiral BNNTs.[13]

We have shown previously that reflection symmetry in a 2D crystal, such as SLBN, leads to a selection rule that forbids any n-phonon scattering process involving an odd number of out-of-plane phonons[17,22] (Appendix A). This selection rule leads to significantly less scattering, especially for ZA phonons, and to higher κ_L. Interlayer coupling and nanotube curvature violate this 2D selection rule causing MLBN and larger-diameter BNNTs to have lower κ_L than SLBN.

III. THERMAL CONDUCTIVITY

We calculate κ_L for BNNTs and MLBN using an exact numerical solution to the phonon Boltzmann transport equation (BTE), previously described elsewhere for SWCNTs,[12,13]

SLBN,[15] graphene,[17,22] and MLG and graphite.[14] Here, we outline this theory. Full details of the phonon BTE and relevant scattering mechanisms can be found in the given references and Appendix B.

The κ_L for each system is given by:

$$\kappa_L = \frac{1}{D} \sum_j \int \left(\partial n_\lambda^0 / \partial T \right) \hbar \omega_\lambda v_{\lambda\alpha}^2 \tau_\lambda d\vec{q}, \qquad (2)$$

where n_λ^0 is the Bose distribution function, α is the Cartesian component in the transport direction, and D is a system-dependent prefactor. For h-BN, Eq. (2) is a 3D integral with $D = (2\pi)^3$. For SLBN and MLBN, Eq. (2) is a 2D integral with $D = (2\pi)^2 N\delta$, where $\delta = 0.333$ nm is the interlayer spacing for h-BN.[3] Since l is quantized for a BNNT wave vector $\vec{q} = (q,l)$, Eq. (2) becomes a 1D integral for q and sum over j and l, while $D = (2\pi)\pi d\delta$, where d is the nanotube diameter. For an infinite 2D hexagonal lattice, the in-plane transport is isotropic and can be represented by a single value, as in Eq. (2). In principle, finite systems display directional anisotropy; though, for the system sizes considered here, this anisotropy is small ($<5\%$) and thus not considered.

In this paper, the phonon lifetimes τ_λ for mode λ are limited by three-phonon, boundary and isotopic impurity scattering. The boundary scattering time, $\tau_\lambda^{bs} = L/2|v_{\lambda\alpha}|$, with L being the length between crystallite or sample boundaries, gives the correct limiting values of κ_L in the ballistic ($L \to 0$) and diffusive ($L \to \infty$) limits for nanotubes and nanoribbons.[27,28] Note, we do not explicitly introduce diffuse scattering from sample sides perpendicular to the transport direction. Such scattering where transport is restricted to 2D layers has recently been shown to be considerably weaker than for the corresponding case of bulk (3D) systems.[29] In any case, for 2D layers, the empirical boundary scattering employed here is closely related to the conventional relation L/v_λ, where $v_\lambda = \sqrt{v_x^2 + v_y^2}$.[15]

The isotopic scattering time τ_λ^{iso} is limited by the large concentration of ^{10}B (19.9%) atoms in the more abundant ^{11}B (80.1%) atoms in naturally occurring boron samples (the nitrogen isotope impurity concentration is negligible). The boron isotopic mass differences are treated as a perturbation to the harmonic Hamiltonian, and the scattering rates are calculated using Fermi's golden rule.[30] For three-phonon interactions, the first anharmonic term in the expansion of the crystal potential is treated as a perturbation to the harmonic phonons. Fermi's golden rule is again used to calculate millions of three-phonon scattering rates, which enter the phonon BTE. The τ_λ are given by the solution of the linearized BTE, which is exactly determined using an iteration process, which accounts for the fact that phonon-phonon scattering couples phonons of different modes. Details of the isotope scattering, three-phonon scattering, and the BTE calculation can be found in Appendix B.

IV. RESULTS AND DISCUSSION

For MLBN, we take the coupled 2D sheets to lie in the x-y plane connecting thermal reservoirs at slightly different temperatures, and we consider thermal transport in the $\Gamma \to M$ direction. We consider boundaries of length L in this transport direction. For BNNTs, we consider zigzag $(n,0)$, armchair (n,n), and chiral (n_1,n_2) BNNTs with diameter d and length L connecting thermal reservoirs. The chiral indices, n_1 and n_2, uniquely identify each BNNT considered. The phase space for three-phonon scattering grows very large with increasing layer number and nanotube diameter in MLBN and BNNTs, respectively. We have been able to calculate the κ_L for MLBN up to $N = 5$ and BNNTs up to $d = 11$ nm. Fully converged κ_L for h-BN was not possible due to the enormous phase space for three-phonon scattering; however, we estimate values to be within 10% of fully converged results.[14] Chiral BNNTs (and zigzag to a lesser extent) have large translational unit cells, and thus large scattering phase spaces, even for relatively small d compared to armchair BNNTs, so calculations of these κ_L are more limited.

Scaled κ_L vs layer number N for MLBN (solid black circles) is shown in Fig. 1 along with the corresponding scaled per branch-type contributions, κ_{ZA}, κ_{TA}, and κ_{LA}, (red/dark gray triangles, green/gray squares, and blue/medium gray diamonds) given by $\kappa_{ZA} = \sum_{i=1}^{N} \kappa_{ZA_i}$, etc. Each system is taken to have length $L = 10$ μm at temperature $T = 300$ K and is scaled by the calculated $\kappa_{SLBN} = 810$ Wm^{-1} K^{-1}. The dashed black line (highest) in Fig. 1 represents the approximate κ_L for h-BN. The dashed red/dark gray, green/gray, and blue/medium gray lines (higher, lower, and lowest) correspond to the per-branch-type values in h-BN. Also shown in Fig. 1 is the calculated κ_L vs N for isotopically pure MLBN (open circles).

Similar to recently published results for MLG,[14] κ_L for MLBN decreases monotonically from a maximum for κ_{SLBN} converging to κ_{hBN} within only a few layers with the largest decrease from SLBN to bilayer BN, $\kappa_{bilayer} = 0.6\kappa_{SLBN}$. The reduction in κ_L for MLBN comes in part from the violation of the 2D selection rule present in SLBN, in part due to lowered density of states of the ZA$_{i>1}$ phonons. As seen in Fig. 1, κ_{ZA} provides the greatest contribution to κ_L for MLBN and drops $\sim$60% from $N = 1$ to $N = 5$, while κ_{TA} and κ_{LA} change little with increasing N. The coupling between layers especially affects the ZA modes, which vibrate perpendicular to the planes. Convergence to κ_{hBN} within only a few layers is a consequence of the limited range of the van der Waals forces. The κ_L for isotopically pure MLBN follows the same trend as κ_L for naturally occurring MLBN with enhancements of 36 and 29% for SLBN and h-BN at room temperature, respectively. In SLBN (and to a lesser extent in MLBN), the isotopic enhancement is sensitive to system size and shows peaks at lower temperature where anharmonic scattering is weaker compared to the boundary and isotope scattering.[15]

To highlight the importance of three-phonon scattering relative to the phonon-isotope scattering in determining κ_L for MLBN around room temperature, we have calculated the ratio $\kappa_L^{iso}/\kappa_L^{pure}$, where κ_L^{iso} is the κ_L determined with only boundary and impurity scattering (natural isotopic composition) and κ_L^{pure} is the κ_L determined with only boundary and three-phonon scattering. We find $\kappa_L^{iso}/\kappa_L^{pure} \sim 4$–10 depending on the system (BNNT, SLBN, or MLBN) and system length ($L = 3$–10 μm). The isotopic scattering is weak compared to three-phonon scattering at $T = 300$ K in h-BN systems, even with high impurity concentrations. This leads to the relatively large values for $\kappa_L^{iso}/\kappa_L^{pure}$.

Furthermore, the κ_L for h-BN systems are significantly lower than for carbon systems.[14,15,17] We demonstrate this by calculating ratios for isotopically pure systems: $\kappa_{\text{graphene}}/\kappa_{\text{SLBN}} \approx 3.2$ and $\kappa_{\text{MLG}}/\kappa_{\text{MLBN}} \approx 3.9$ for similar layer number. The small difference in the ratios may come from stronger anharmonic scattering in MLBN due to slightly smaller interlayer spacing and different stacking orientation compared to MLG. To gain further insights into the reduced κ_L of h-BN systems compared to carbon systems, we have developed hypothetical models which mix different aspects (frequencies, velocities, anharmonic IFCs, etc.) of isotopically pure MLG and MLBN in the BTE calculations. This was recently done with MD simulations of SLBN;[10] however, anharmonic effects on the phonon scattering times of the different systems were not considered. We find that the main cause for the reduction of κ_L in SLBN and MLBN compared to graphene and MLG comes from stronger three-phonon scattering rates due to the somewhat lower phonon frequencies in the h-BN systems. The scattering rates, Eq. (B4), are strongly dependent on these frequencies since they enter inversely directly and through the Bose factors. Thus, the reduced frequencies substantially increase the scattering rates and lower κ_L.

We now consider the nanotubes. Figure 2 shows the scaled κ_L vs diameter d for a series of naturally occurring isotopic composition armchair (black circles), zigzag (black triangles), and chiral (black squares) BNNTs with length $L = 3\ \mu$m at temperature $T = 300$ K. The κ_L are scaled by the calculated $\kappa_{\text{SLBN}} = 650\ \text{Wm}^{-1}\ \text{K}^{-1}$ [indicated by the black line (highest)].
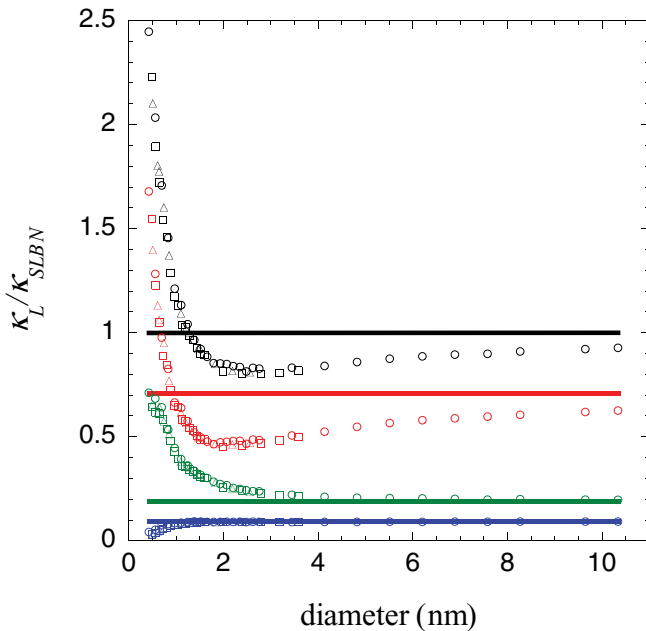
In Fig. 2, the contributions κ_j to κ_L of BNNTs for each branch $j = 1,2$, and 3 (obtained by summing over all of the l values) are given by the colored symbols [red/dark gray (higher), $j = 1$; green/gray (lower), $j = 2$; and blue/medium gray (lowest), $j = 3$] along with the corresponding colored lines for the per-branch contributions to κ_{SLBN} [red/dark gray (higher), ZA; green/gray (lower), TA; blue/medium gray (lowest), LA]. The κ_j for large d nanotubes converge to their corresponding κ_{SLBN} counterparts: $\kappa_1 \rightarrow \kappa_{\text{ZA}}$, $\kappa_2 \rightarrow \kappa_{\text{TA}}$, and $\kappa_3 \rightarrow \kappa_{\text{LA}}$.

The nonmonotonic behavior of the κ_L vs d curve is a consequence of the competition between the onset of the 2D scattering selection rule for large d BNNTs and the loss of optic scattering channels for small d BNNTs. For large d, where the nanotube curvature is small, the 2D selection rule is well approximated and $\kappa_L \approx \kappa_{\text{SLBN}}$. As d decreases, the nanotube curvature increasingly violates the 2D selection rule, leading to stronger scattering of the out-of-tube phonons and reduction of κ_1 and κ_L. Note that κ_2 and κ_3 change very little for the larger-diameter nanotubes because the in-tube modes, which correspond to the TA and LA modes in SLBN, are little affected by the 2D selection rule. The κ_L has a minimum for $d \sim 3$ nm where quantization effects in the nanotubes begin to play a more significant role. As d decreases, the number of optic phonon modes decreases and are pushed to higher frequencies. Thus, the optic phonons become less efficient scatterers of the lower-lying acoustic phonons, especially for $j = 1$ and 2, which leads to increased κ_L.

Figure 3 shows the κ_L vs T for a (10,10) BNNT (black; lower) and a (10,10) SWCNT (red/dark gray; upper) with $L = 3\ \mu$m. The dashed curves correspond to isotopically pure ^{11}B and ^{12}C, and the solid curves correspond to naturally

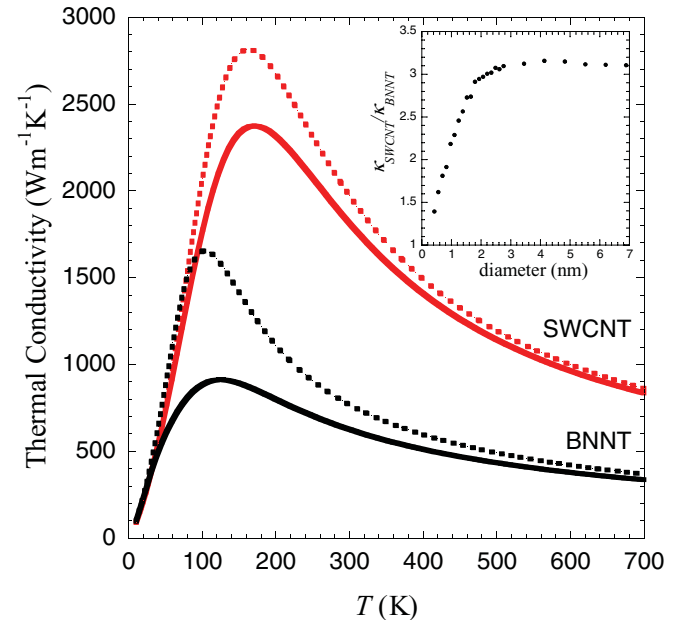FIG. 2. (Color online) Here, κ_L and branch contributions to κ_L summed over l for each j vs d for a variety of zigzag (triangles), armchair (circles), and chiral (squares) BNNTs. $j = 1, 2, 3$ and total correspond to red/dark gray (higher), green/gray (lower), blue/medium gray (lowest), and black shapes (highest), respectively. The horizontal lines show the associated contributions to κ_{SLBN} for the ZA, TA, and LA modes as well as the total. For all cases, $L = 3\ \mu$m and $T = 300$ K.

FIG. 3. (Color online) Calculated κ_L vs T for a (10,10) SWCNT (red/dark gray; upper) and a (10,10) BNNT (black; lower) with isotopically pure (dashed) and naturally occurring (solid) carbon and boron abundances. For all cases, $L = 3\ \mu$m. The inset shows $\kappa_{\text{SWCNT}}/\kappa_{\text{BNNT}}$ vs d for similar isotopically pure armchair nanotubes with $T = 300$ K.

occurring boron and carbon abundances [^{10}B (19.9%) and ^{13}C (1.1%)]. For temperatures above about 100 K, the behavior of κ_L is governed by phonon-phonon scattering and phonon-isotope scattering. In this temperature range, the κ_L for both naturally occurring and isotopically enriched BNNTs lie well below those for the SWCNTs. This reflects the stronger phonon-phonon scattering rates in the former. This is further demonstrated by the lower temperatures of the peaks in κ_L for the BNNTs ($T \sim 100$ K) compared to the SWCNTS ($T \sim 150$ K). For T below the peak temperature, κ_L decreases as boundary scattering provides the dominant resistance. For low T, only low-frequency phonons are thermally populated and can contribute to thermal transport and resistance. The out-of-tube ($j = 1$) phonon branch contributions to κ_L dominate in this temperature regime because of the high density of phonon modes at low frequencies. For T above the peak temperature, κ_L drops with increasing T, which is a signature that phonon-phonon scattering is stronger than the phonon-isotope scattering and boundary scattering. At $T = 300$ K, we find that the ratio of κ_L for a natural isotopic composition (10,10) SWCNT and an isotopically pure (10,10) BNNT is $\kappa_{\text{SWCNT}}/\kappa_{\text{BNNT}} = 2.3$. The inset to Fig. 3 shows the ratio $\kappa_{\text{SWCNT}}/\kappa_{\text{BNNT}}$ vs d for similar isotopically pure armchair SWCNTs and BNNTs with $L = 3$ μm and $T = 300$ K. For small d, $\kappa_{\text{SWCNT}}/\kappa_{\text{BNNT}} \approx 1.5$. This ratio increases with diameter and saturates to ~ 3 for the larger nanotubes, where optic modes provide a significant amount of scattering and the 2D selection rule plays a role.

Figure 4 plots the percent enhancement to κ_L, $P = (\kappa_L^{\text{pure}}/\kappa_L^{\text{nat}} - 1) \times 100\%$, from isotopic enrichment as a function of temperature for the (10,10) BNNTs (black solid curve) and (10,10) SWCNTs (red/dark gray dashed curve) with $L = 3$ μm. For T decreasing from room temperature, P increases in both systems, reflecting the weakening of the phonon-phonon
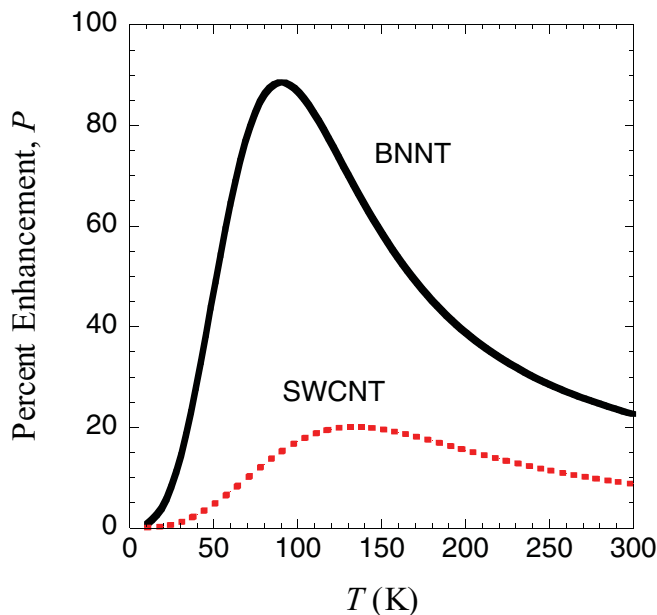

FIG. 4. (Color online) Isotope enhancement factor P as a function of temperature for BNNTs (black solid curve) and SWCNTs (red dashed curve).

scattering due to freeze-out of Umklapp processes. At $T = 300$ K, $P = 23\%$ for BNNTs and $P = 9\%$ for SWCNTs, while at the temperatures giving the peaks in κ_L, $P = 89$ and 20%, respectively. Since phonon-phonon scattering is stronger in BNNTs, a much larger P enhancement for BNNTs is evident. The overall larger P for BNNTs is a consequence of the larger isotope scattering resulting from the much higher isotope concentration. Given the small ($\sim 1\%$) ^{13}C concentration in naturally occurring SWCNTs, the relatively large isotope effect arises because of the comparably weak phonon-phonon scattering. Finally, we note that the peak value increases rather strongly with increasing nanotube length, as has been noted previously for SLBN.[15]

To summarize these results, for all of the nanotubes considered here $\kappa_{\text{SWCNT}} > \kappa_{\text{BNNT}}$, which is largely due to the stronger anharmonic phonon scattering in the BNNTs rather than the stronger isotope scattering. This is qualitatively similar to SLBN and MLBN systems discussed above. Furthermore, we find a strong temperature dependence to the enhancement factor P, a feature that has been commonly observed previously in bulk semiconductors.[31–33] Recent measurements[11] have found room temperature isotopic enhancement in κ_L of $P \sim 50\%$, which is somewhat larger than our calculated value. Since scattering of phonons by isotopes is well represented within the BTE approach,[34] then accepting the experimental number would suggest that our anharmonic scattering rates are too large. On the other hand, the measured isotopic enhancement in Ref. 11 is roughly temperature independent, which suggests such weak anharmonic scattering that the κ_L for bulk h-BN would be far higher than measured.[8] Finally, we note that the room temperature κ_L for multiwalled carbon nanotubes ($\kappa_L = 320$ Wm^{-1} K^{-1}) reported in Ref. 11 are below those found previously ($\kappa_L = 2000$–3000 Wm^{-1} K^{-1}),[35,36] although Ref. 11 points out a known error in these earlier measurements associated with lack of transmission electron microscopy characterization. Perhaps more importantly, the value quoted in Ref. 11 is seven times lower than that of bulk pyrolytic graphite.[9] Ultimately, further research on the κ_L for naturally occurring and isotopically enriched carbon and boron nitride nanotubes are needed to address this issue.

Here, we will compare our phonon BTE results for the κ_L of BNNTs with those of recent theoretical work. Reference 37 was able to match the temperature independence of the isotopic enhancment of κ_L for multiwalled BNNTs measured in Ref. 11, but this required assuming a very weak phonon-phonon scattering so that the phonon-isotope scattering is dominant. In contrast, around room temperature, we find three-phonon scattering is stronger than isotopic impurity scattering, a characteristic seen in bulk h-BN where κ_L decreases with temperature around 300 K, a sign that anharmonic scattering is dominant, as in most semiconductors.

In Ref. 10 (MD simulation) and Ref. 38 (kinetic theory), isotopic impurity scattering is ignored, while the focus is on phonon-phonon scattering in limiting κ_L for small-diameter BNNTs ($d \sim 0.4$–1.4 nm). Like these works, we find lower κ_L for BNNTs than for SWCNTs (though for a more expansive range of diameters), which we attribute to stronger anharmonic three-phonon scattering, especially for moderate to large diameter BNNTs. As in Ref. 38, we find strong contributions from the quadratic ($l = \pm 1$, $j = 1$) acoustic modes for small

diameter BNNTs. In larger BNNTs, we demonstrate that all of the $j = 1$ modes for different l's (out-of-tube vibrations) combine to make a strong contribution to κ_L, which we connect to the approximation of a 2D selection rule in a flat SLBN sheet. Finally, here, we have presented a theory and results for the full solution of the phonon BTE without use of the single-mode relaxation time approximation (RTA) that is used in Ref. [38], which misses important aspects of thermal transport in h-BN systems. For example, while the proper azimuthal symmetries are taken into account in Ref. [38], normal scattering is incorrectly treated as independently resistive. Also, extending this RTA to larger BNNTs with smaller tube curvature will fail due to the role of the 2D selection rule.

Finally, we highlight the importance of implementing a full solution of the BTE that includes both normal and resistive Umklapp scattering processes. Low-frequency, zone-center phonons participate very little in Umklapp scattering but have very strong normal scattering channels, which are not themselves resistant to a thermal current. However, the normal scattering processes are important for redistributing these low-frequency phonons to higher frequencies away from the Brillouin zone center, where they can undergo Umklapp scattering and thus encounter thermal resistance. We find this born out in the iterative solution to the BTE, similar to SWCNTs.[12] Let us consider an isotopically pure (10,10) BNNT with $L = 3$ μm and $T = 300$ K which has $\kappa_L = 769$ Wm^{-1} K^{-1}. Neglecting Umklapp scattering processes, the zeroth-order BTE solution (relaxation time approximation) gives $\kappa_L = 426$ Wm^{-1} K^{-1}, which is qualitatively wrong because normal processes alone cannot provide resistance. However, upon iteration, the phonon lifetimes diverge, which leads to divergent κ_L. Neglecting normal scattering processes leads to a converged $\kappa_L = 4937$ Wm^{-1} K^{-1}, which is significantly higher than the full solution, demonstrating the importance of both normal and Umklapp processes in determining κ_L.

V. SUMMARY AND CONCLUSIONS

The κ_L of BNNTs and MLBN have been calculated, using an exact numerical solution of the phonon BTE. This theoretical approach highlights the large contributions from out-of-tube vibrations in BNNTs and out-of-plane vibrations in MLBN. Such contributions are shown to be smaller in larger-diameter BNNTs and in MLBN than in SLBN due to the breaking of a 2D selection rule from nanotube curvature and interlayer coupling, respectively. The κ_L for MLBN decreases monotonically from SLBN with increasing number of layers and converges to κ_L for h-BN within a few layers. For differing chirality BNNTs, κ_L exhibits a nonmonotonic diameter dependence and converges to the κ_L of SLBN for large d nanotubes due to vanishing curvature and recovery of the 2D selection rule in SLBN. We also show that, around room temperature, anharmonic phonon scattering is the dominant mechanism limiting κ_L and is responsible for the lower κ_L in BNNTs and MLBN compared to SWCNTs and MLG despite large isotopic impurity scattering. We have shown that BNNTs have a temperature-dependent isotope effect with large enhancements to κ_L for isotopically pure BNNTs despite stronger phonon-phonon scattering.

ACKNOWLEDGMENTS

APPENDIX A

1. Azimuthal selection rule for BNNTs

There are two momentum selection rules for BNNTs with chiral indices (n_1, n_2):[12,13,18]

$$q \pm q' = q'' + K, \quad l \pm l' = (l'' + l_K) \bmod [g], \quad \text{(A1)}$$

where q is the wave vector along the nanotube axis, $-\pi/a < q < \pi/a$, a is the length of the unit cell, l is the angular quantum number which takes on the integer values $l = 0, \pm 1, \ldots + g/2$, and K is a reciprocal lattice vector. Here, $g = 2(n_1^2 + n_1 n_2 + n_2^2)/n_{\text{gcd}}\chi$ is the number of two-atom unit cells in the translational unit cell of each BNNT where n_{gcd} is the greatest common divisor of n_1 and n_2, and $\chi = 3$ if $(n_1 - n_2)/3 n_{\text{gcd}}$ is an integer; otherwise, $\chi = 1$.[39–41] Note that g reduces to $2n$ for armchair (n,n) and zigzag $(n,0)$ BNNTs. In, Eq. (A1), the mod function keeps $l'' + l_K$ between $-g/2 + 1$ and $g/2$. For normal scattering processes, $K = l_K = 0$. For Umklapp scattering processes, $K = \pm 2\pi/a$ and the integer $l_K = \pm p$, where p is given by:[13,39–41]

$$p = g\, \text{Fr}\left[\frac{n_{\text{gcd}}\chi}{g(2n_1 + n_2)} \left\{ g\left(\frac{n_1 + 2n_2}{n_{\text{gcd}}\chi}\right)^{\phi[(2n_1+n_2)/n_{\text{gcd}}\chi]-1} - n_2 \right\} \right], \quad \text{(A2)}$$

where $\text{Fr}[x]$ is the fractional part of the rational number x, and $\phi[y]$ is the Euler function. For armchair and zigzag BNNTs $p = n$.

2. 2D selection rule for SLBN

For strictly 2D systems, such as SLBN, a selection rule on phonon-phonon scattering arises from reflection symmetry of the lattice potential energy Φ with respect to its equilibrium value:[17,22]

$$\Phi(\ldots \vec{r}_{\ell_i \kappa_i} \ldots) = \sum_{n=2}^{\infty} \frac{1}{n} \sum_{\ell_1 \kappa_1, \ldots, \ell_n \kappa_n} \sum_{\alpha_1, \ldots, \alpha_n} \Phi_{\alpha_1 \ldots \alpha_n}(\ell_1 \kappa_1; \ldots; \ell_n \kappa_n)$$
$$\times u_{\alpha_1}(\ell_1 \kappa_1) \ldots u_{\alpha_n}(\ell_n \kappa_n). \quad \text{(A3)}$$

Here, $\vec{r}_{\ell\kappa} = \vec{R}_{\ell\kappa} + \vec{u}_{\ell\kappa}$ specifies the instantaneous location of the κth atom in the ℓth unit cell, $\vec{R}_{\ell\kappa}$ and

$\vec{u}_{\ell\kappa}$ give the equilibrium position and the displacement from equilibrium, and α_i are Cartesian components. The nth order interatomic force constants (IFCs) are given by: $\Phi_{\alpha_1...\alpha_n}(\ell_1\kappa_1;...\ell_n\kappa_n) = \frac{\partial^n \Phi}{\partial u_1(\ell_1\kappa_1)...\partial u_n(\ell_n\kappa_n)}|_0$, where the derivative is evaluated at the equilibrium lattice positions. In Eq. (A3), the $n = 2$ term gives the harmonic potential energy, while the $n = 3$ term leads to three-phonon scattering.

The potential energy must be invariant under the symmetry operations of the lattice.[42] Equating like terms in the expanded potential before and after the z-axis reflection operation on a 2D lattice lying in the x-y plane leads to the following condition:[17,22]

$$\Phi_{\alpha_1...\alpha_n}(\ell_1\kappa_1;...;\ell_n\kappa_n) = 0, \quad m \text{ odd}, \quad (A4)$$

where m is the number of z components in the string, $\alpha_1 ... \alpha_n$. This condition constrains the IFCs for all orders; in particular, third-order IFCs such as $\Phi_{zzz}(\ell_1\kappa_1; \ell_2\kappa_2; l_3\kappa_3)$ must vanish. In SLBN, only even numbers of out-of-plane (z component) phonons can be involved in a three-phonon scattering process, which leads to severe phase space limitations and enhanced κ_L.

APPENDIX B

1. Phonon boltzmann transport equation

The BTE is a set of coupled equations for the phonon lifetimes τ_λ:[12–15,17]

$$\tau_\lambda = \tau_\lambda^0(1 + \Delta_\lambda), \quad (B1)$$

where τ_0 are phonon lifetimes within the relaxation time approximation, given by:

$$1/\tau_\lambda^0 \equiv \sum_{\lambda',\lambda''}{}^{(+)}\Gamma_{\lambda\lambda'\lambda''}^{(+)} + 1/2\sum_{\lambda',\lambda''}{}^{(-)}\Gamma_{\lambda\lambda'\lambda''}^{(-)} + 1/\tau_\lambda^{bs} + 1/\tau_\lambda^{iso},$$

$$(B2)$$

where the sums are over the scattering phase space for processes that satisfy the conservation conditions and the $\pm$ corresponds to the two possible types of three-phonon processes.[16] Here, $\tau_\lambda^{bs} = L/2|v_{\lambda\alpha}|$ is the boundary scattering time and τ_λ^{iso} is the scattering time due to isotopic impurities given by:[30]

$$1/\tau_\lambda^{iso} = \frac{\pi}{2}\frac{\Omega}{(2\pi)^x}\omega_\lambda^2\sum_{j'\kappa}g_\kappa\int d\vec{q}' |e_{\kappa\lambda}e_{\kappa\lambda'}^*|^2\delta(\omega_\lambda - \omega_{\lambda'}),$$

$$(B3)$$

where Ω is the unit cell volume and $e_{\kappa\lambda}$ is the eigenvector for the κth atom in mode λ. The integral is 1D, 2D, or 3D

with $x = 1$, 2, or 3 for BNNTs, SLBN and MLBN, and h-BN, respectively. In Eq. (B3), $g_\kappa = \frac{1}{\bar{m}_\kappa^2}\sum_i f_{i\kappa}(m_{i\kappa} - \bar{m}_\kappa)^2$, is a mass variance parameter with $f_{i\kappa}$ and $m_{i\kappa}$ being the concentration and the mass of the ith isotope of the κth atom, and $\bar{m}_\kappa$ being the average mass. For boron atoms $g_B = 1.366 \times 10^{-3}$, and we take $g_N = 0$ for nitrogen atoms. The isotope scattering is treated here in the relaxation time approximation. In principle, this scattering can also enter the iteration process.[43,44] However, we find that this does not change the resulting κ_L.

The $\Gamma_{\lambda\lambda'\lambda''}^{(\pm)}$ in Eq. (B2) are intrinsic anharmonic scattering rates determined via Fermi's golden rule for three-phonon scattering:[12–15,17]

$$\Gamma_{\lambda\lambda'\lambda''}^{(\pm)} = \frac{\hbar\pi}{4N_0\omega_\lambda\omega_{\lambda'}\omega_{\lambda''}}\left\{\begin{array}{c}n_{\lambda'}^0 - n_{\lambda''}^0 \\ n_{\lambda'}^0 + n_{\lambda''}^0 + 1\end{array}\right\}|\Phi_{\lambda,\pm\lambda',-\lambda''}^{(\pm)}|^2\delta(\omega_\lambda$$

$$\pm \omega_{\lambda'} - \omega_{\lambda''}) \quad (B4)$$

with matrix elements:

$$\Phi_{\lambda\lambda'\lambda''} = \sum_\kappa\sum_{l'\kappa'}\sum_{l''\kappa''}\sum_{\alpha\beta\gamma}\Phi_{\alpha\beta\gamma}(0\kappa,l'\kappa',l''\kappa'')$$

$$\times \frac{e_{\alpha\kappa}^\lambda e_{\beta\kappa'}^{\lambda'} e_{\gamma\kappa''}^{\lambda''}}{\sqrt{m_\kappa m_{\kappa'} m_{\kappa''}}}e^{i\vec{q}'\vec{R}_{l'}}e^{i\vec{q}''\vec{R}_{l''}}, \quad (B5)$$

where $\Phi_{\alpha\beta\gamma}(0\kappa,l'\kappa',l''\kappa'')$ are third-order anharmonic IFCs, the $e_{\alpha\kappa}^\lambda$ are phonon eigenvectors, N_0 is the number of unit cells in the crystal, and $-\lambda \Rightarrow (-\vec{q}, j)$. In Eq. (B1), Δ_λ is an inelastic mode coupling term given by:

$$\Delta_\lambda = \sum_{\lambda'\lambda''}{}^{(+)}\Gamma_{\lambda\lambda'\lambda''}^{(+)}(\xi_{\lambda\lambda''}\tau_{\lambda''} - \xi_{\lambda\lambda'}\tau_{\lambda'})$$

$$+ \frac{1}{2}\sum_{\lambda'\lambda''}{}^{(-)}\Gamma_{\lambda\lambda'\lambda''}^{(-)}(\xi_{\lambda\lambda''}\tau_{\lambda''} + \xi_{\lambda\lambda'}\tau_{\lambda'}), \quad (B6)$$

where $\xi_{\lambda\lambda'} = v_{\lambda'}\omega_{\lambda'}/v_\lambda\omega_\lambda$.

A grid of points is defined throughout the Brillouin zone and for each λ on the grid, the phase space of λ', λ'' is found numerically using a root-finding algorithm. The boundary, isotopic impurity, and anharmonic scattering rates are calculated from Eqs. (B3) and (B4), which allows determination of τ_λ^0 (RTA) from Eq. (B2), $\Delta_\lambda = 0$. The full solution to the BTE with $\Delta_\lambda \neq 0$ is found using an iterative scheme where $\tau_\lambda^{(0)} = \tau_\lambda^0$ is the zeroth iteration. Plugging this into Eqs. (B1) and (B6) yields $\tau_\lambda^{(1)}$. The iteration scheme is continued until the calculated κ_L from Eq. (2) differs negligibly on successive iterations.

---

*Corresponding author: lucas.lindsay.ctr@nrl.navy.mil

[1]G. A. Slack, Phys. Rev. **127**, 694 (1962).

[2]K. Watanabe, T. Taniguchi, and H. Kanda, Nat. Mater. **3**, 404 (2004).

[3]W. Paszkowicz, J. B. Pelka, M. Knapp, T. Szyszko, and S. Podsiadlo, Appl. Phys. A **75**, 431 (2001).

[4]R. Nicklow, N. Wakabayashi, and H. G. Smith, Phys. Rev. B **5**, 4951 (1972).

[5]J. Maultzsch, S. Reich, C. Thomsen, H. Requardt, and P. Ordejón, Phys. Rev. Lett. **92**, 075501 (2004).

[6]M. Mohr, J. Maultzsch, E. Dobardžić, S. Reich, I. Milošević, M. Damnjanović, A. Bosak, M. Krisch, and C. Thomsen, Phys. Rev. B **76**, 035439 (2007).

[7]J. Serrano, A. Bosak, R. Arenal, M. Krisch, K. Watanabe, T. Taniguchi, H. Kanda, A. Rubio, and L. Wirtz, Phys. Rev. Lett. **98**, 095503 (2007).

[8]E. K. Sichel, R. E. Miller, M. S. Abrahams, and C. J. Buiocchi, Phys. Rev. B **13**, 4607 (1976).

[9]G. A. Slack, Phys. Rev. **127**, 694 (1962).

[10]C. Sevik, A. Kinaci, J. B. Haskins, and T. Çağin, Phys. Rev. B **84**, 085409 (2011).

[11]C. W. Chang, A. M. Fennimore, A. Afanasiev, D. Okawa, T. Ikuno, H. Garcia, Deyu Li, A. Majumdar, and A. Zettl, Phys. Rev. Lett. **97**, 085901 (2006).

[12]L. Lindsay, D. A. Broido, and N. Mingo, Phys. Rev. B **80**, 125407 (2009).

[13]L. Lindsay, D. A. Broido, and N. Mingo, Phys. Rev. B **82**, 161402(R) (2010).

[14]L. Lindsay, D. A. Broido, and N. Mingo, Phys. Rev. B **83**, 235428 (2011).

[15]L. Lindsay and D. A. Broido, Phys. Rev. B **84**, 155421 (2011).

[16]J. M. Ziman, *Electrons and Phonons* (Oxford University Press, London, 1960), p. 288.

[17]L. Lindsay, D. A. Broido, and N. Mingo, Phys. Rev. B **82**, 115427 (2010).

[18]V. N. Popov, V. E. Van Doren, and M. Balkanski, Phys. Rev. B **61**, 3078 (2000).

[19]N. Marom, J. Bernstein, J. Garel, A. Tkatchenko, E. Joselevich, L. Kronik, and O. Hod, Phys. Rev. Lett. **105**, 046801 (2010).

[20]J. Tersoff, Phys. Rev. Lett. **61**, 2879 (1988).

[21]J. Tersoff, Phys. Rev. B **37**, 6991 (1988).

[22]J. H. Seol, I. Jo, A. L. Moore, L. Lindsay, Z. H. Aitken, M. T. Pettes, X. Li, Z. Yao, R. Huang, D. A. Broido, N. Mingo, R. S. Ruoff, and L. Shi, Science **328**, 213 (2010).

[23]D. Donadio and G. Galli, Phys. Rev. Lett. **99**, 255502 (2007).

[24]S. Berber, Y. K. Kwon, and D. Tománek, Phys. Rev. Lett. **84**, 4613 (2000).

[25]L. Lindsay and D. A. Broido, Phys. Rev. B **81**, 205441 (2010).

[26]K. H. Michel and B. Verberck, Phys. Rev. B **83**, 115328 (2011).

[27]N. Mingo and D. A. Broido, Nano Lett. **5**, 1221 (2005).

[28]E. Munoz, J. Lu, and B. Yakobson, Nano Lett. **10**, 1652 (2010).

[29]Z. Wang and N. Mingo, Appl. Phys. Lett. **99**, 101903 (2011).

[30]S. I. Tamura, Phys. Rev. B **27**, 858 (1983).

[31]L. Wei, P. K. Kuo, R. L. Thomas, T. R. Anthony, and W. F. Banholzer, Phys. Rev. Lett. **70**, 3764 (1993).

[32]V. Inyushkin, A. N. Taldenkov, A. M. Gibin, A. V. Gusev, and H.-J. Pohl, Phys. Status Solidi C **1**, 2995 (2004).

[33]M. Asen-Palmer, K. Bartkowski, E. Gmelin, M. Cardona, A. P. Zhernov, A. V. Inyushkin, A. Taldenkov, V. I. Ozhogin, K. M. Itoh, and E. E. Haller, Phys. Rev. B **56**, 9431 (1997).

[34]G Stoltz, M Lazzeri, and F Mauri, J. Phys. Condens. Matter **21**, 345302 (2009).

[35]P. Kim, L. Shi, A. Majumdar, and P. L. McEuen, Phys. Rev. Lett. **87**, 215502 (2001).

[36]M. Fujii, X. Zhang, H. Xie, H. Ago, K Takahashi, T. Ikuta, H. Abe, and T. Shimizu, Phys. Rev. Lett. **95**, 065502 (2005).

[37]D. A. Stewart, I. Savić, and N. Mingo Nano Lett. **9**, 81 (2009).

[38]J. W. Jiang and J. S. Wang, Phys. Rev. B **84**, 085439 (2011).

[39]S. Reich, C. Thomsen, and J. Maultzsch, *Carbon Nanotubes: Basic Concepts and Physical Properties*, (Wiley-VCH, Weinheim, 2004), p. 3.

[40]N. Bozovic, I. Bozovic, and M. Damnjanovic, J. Phys. A **18**, 923 (1985); **17**, 747 (1984).

[41]R. A. Jishi, M. S. Dresselhaus, and G. Dresselhaus, Phys. Rev. B **47**, 16671 (1993).

[42]G. Leibfried and W. Ludwig, Solid State Phys. **12**, 275 (1961).

[43]M. Omini and A. Sparavigna, Nuovo Cimento D **19**, 1537 (1997).

[44]D. A. Broido, A. Ward, and N. Mingo, Phys. Rev. B **72**, 014308 (2005).